Journal of Solid State Chemistry 182 (2009) 471–478

Contents lists available at ScienceDirect

Journal of Solid State Chemistry

journal homepage: www.elsevier.com/locate/jssc

Syntheses, crystal structures and spectroscopic properties of $Ag_2Nb[P_2S_6][S_2]$ and $KAg_2[PS_4]$

Yuandong Wu, Wolfgang Bensch *

Institut für Anorganische Chemie, Universität Kiel, Olshausenstr. 40, D-24098 Kiel, Germany

ARTICLE INFO

Article history:
Received 5 September 2008
Received in revised form
28 October 2008
Accepted 2 November 2008
Available online 21 November 2008

Keywords:
Silver
Thiophosphates
Crystal structure
Spectroscopic properties

ABSTRACT

$Ag_2Nb[P_2S_6][S_2]$ (**1**) was obtained from the direct solid state reaction of Ag, Nb, P_2S_5 and S at 500 °C. $KAg_2[PS_4]$ (**2**) was prepared from the reaction of K_2S_3, Ag, Nd, P_2S_5 and extra S powder at 700 °C. Compound **1** crystallizes in the orthorhombic space group *Pnma* with $a = 12.2188(11)$, $b = 26.3725(16)$, $c = 6.7517(4)$ Å, $V = 2175.7(3)$ Å^3, $Z = 8$. Compound **2** crystallizes in the non-centrosymmetric tetragonal space group $I\bar{4}2m$ with lattice parameters $a = 6.6471(7)$, $c = 8.1693(11)$ Å, $V = 360.95(7)$ Å^3, $Z = 2$. The structure of $Ag_2Nb[P_2S_6][S_2]$ (**1**) consists of $[Nb_2S_{12}]$, $[P_2S_6]$ and new found puckered $[Ag_2S_4]$ chains which are along [001] direction. The Nb atoms are located at the center of distorted bicapped trigonal prisms. Two prisms share square face of two $[S_2^{2-}]$ to form one $[Nb_2S_{12}]$ unit, in which Nb–Nb bond is formed. The $[Nb_2S_{12}]$ units share all S^{2-} corners with ethane-like $[P_2S_6]$ units to form 14-membered rings. The novel puckered $[Ag_2S_4]$ chains are composed of distorted $[AgS_4]$ tetrahedra and $[AgS_3]$ triangles that share corners with each other. These chains are connected with $[P_2S_6]$ units and $[Nb_2S_{12}]$ units to form three-dimensional frame work. The structural skeleton of **2** is built up from $[AgS_4]$ and $[PS_4]$ tetrahedra linked by corner-sharing. The three-dimensional anionic framework contains orthogonal, intersecting tunnels directed along [100] and [010]. This compound possesses a compressed chalcopyrite-like structure. The structure is compressed along [001] and results from eight coordination sphere for K^+. Both compounds are characterized with UV/vis diffuse reflectance spectroscopy and compound **1** with IR and Raman spectra.

1. Introduction

Transition metal thiophosphates form a wide and interesting class of compounds that has been the subject of numerous investigations because of their broad structural variety [1] and their physical properties. Well-known examples of transition metal thiophosphates include layered MPS_3 (M = Cd, Zn, Mn, Fe, Co, Ni, Hg, Mg, Ca, V, Pd, Sn) [2–9] and mixed metal derivatives $AgMP_2S_6$ (M = Sc, V, Cr, In, Bi) [10–14], $Ag_2MP_2S_6$ (M = Mg, Mn, Zn) [15–18], $AgZnPS_4$ [19], $Ag_2Ti_2P_2S_{11}$ [20], $AgTi_2[PS_4]_3$ and $Ag_2NbTi_3P_6S_{25}$ [21], ANb_2PS_{10} (A = Na, Ag) [22]. The ethane-like $[P_2S_6]$ unit is the common building block in most of these compounds. In the MPS_3 or $M_2P_2S_6$ families, the stability of the transition metal in the 2+ oxidation state decreases from Zn to Ti. Besides these divalent metals, trivalent metals were found to form $M_4[P_2S_6]_3$ (M = Cr, In, Ga) [23–25], which crystallize in a metal-deficient three-fold superstructure of the $Fe_2P_2S_6$ type. In the vanadium case, the most stable phase is a mixed valence phase $V_{0.78}PS_3$ [26]. The V(III), Cr(III) and In(III) compounds can be isolated if one is substituted by Cu or Ag cations. Phases such as $CuMP_2S_6$ (M = V, Cr, In) [27–31] are obtained, whereas different stoichiometries are observed with larger alkali cations, for example, $NaV_{1-x}P_2S_6$ [32], $NaCrP_2S_6$ [33], AMP_2S_7 (A = K, Rb, Cs; M = Cr, V, In) [34–36], $K_4VP_2S_9$ [37], $A_3Cr_2[PS_4]_3$ (A = Na, K) [38,39]. The explorative investigation of rare earth(III) chalcogophosphates revealed a fascinating variety of many quaternary compounds with structures ranging from isolated ions to three-dimensional networks [40]. In the neodymium case, six thiophosphates $Li_9Nd_2[PS_4]_5$ [41], $K_2NdP_2S_7$ [42], $K_9Nd[PS_4]_4$, $A_3Nd[PS_4]_2$ (A = K, Cs) and $K_3Nd_3[PS_4]_4$ [40] are observed. For the heavier homologue of V, the $M_2P_2S_6$ structural model is not observed and niobium is present as Nb^{4+} in Nb_2PS_{10} [43], $Nb_4P_2S_{21}$ [44], NbP_2S_8 [45,46], which present different two-dimensional structural patterns containing $[Nb_2S_{12}]$ units. The Nb atoms are centered in distorted bicapped trigonal prismatic polyhedra, and neighboring polyhedra share square faces and edges forming Nb–Nb pairs. The intercalation of alkali and silver into such structures breaks the –S–S– or –S–S–S– bridges between the one-dimensional chains to form ANb_2PS_{10} (A = Na, Ag, K, Rb, Cs) [22,47–50], $K_{0.5}Ag_{0.5}Nb_2PS_{10}$ [51], $Rb_{0.38}Ag_{0.5}Nb_2PS_{10}$ [52], $K_{0.34}Cu_{0.5}Nb_2PS_{10}$ [53] and $Rb_2Nb_2P_2S_{11}$ [54]. Alkali and silver cations reside in exactly the same site in the van der Waals gap between infinite

* Corresponding author. Fax: +49 431 880 1520.
E-mail address: wbensch@ac.uni-kiel.de (W. Bensch).

0022-4596/$ - see front matter © 2008 Elsevier Inc. All rights reserved.
doi:10.1016/j.jssc.2008.11.017

chains. To stabilize the Nb(IV), we choose Ag(I) as counter-cation. This choice was done according to the interesting specific characteristics of Ag(I), e.g., abnormally high atomic displacement parameters, a preference for low coordination environments and tendency to form d^{10}–d^{10} homo-atomic bonds when their concentration is large [55]. Some detailed spectroscopic and crystallographic investigations [3,56] have clearly demonstrated the unusually large atomic displacement parameters for d^{10} cations derived from a static disorder produced by off-center displacements.

The aims of the present study were the syntheses and characterization of new Ag(I) containing thiophosphates. The results of the X-ray diffraction experiments should yield more information about the behavior of Ag(I) in such thiophosphate phases. In the manuscript we present the synthesis, structural and optical characterization of new quaternary compounds $Ag_2Nb[P_2S_6][S_2]$ and $KAg_2[PS_4]$.

2. Experimental

2.1. Reagents

The following reagents were used as purchased: K (99.5%, Strem), Nb (99.97%, Fluka), P_2S_5 (99.99% purity, Alfa), S (99.99%, Heraeus), Ag (99.99%, Degussa), Nd (99.99%, Alfa Aesar).

2.2. Synthesis

K_2S_3 was prepared from a stoichiometric mixture of the elements in liquid ammonia under an argon atmosphere.

2.2.1. Preparation of $Ag_2Nb[P_2S_6][S_2]$(**1**)

$Ag_2Nb[P_2S_6][S_2]$ (**1**) was prepared by the reaction of a mixture of 0.0664 g (0.62 mmol) of Ag, 0.0572 g (0.62 mmol) of Nb, 0.1369 g (0.62 mmol) of P_2S_5 and 0.0395 g (1.23 mmol) of S. The mixture was loaded in a fused silica tube which was then flame-sealed under vacuum ($\sim 10^{-3}$ mbar). The mixture was annealed at 500 °C for 6 days, followed by cooling to 100 °C at a rate of 2 °C/h. The product contained red crystals (60% yield based on Nb).

2.2.2. Preparation of $KAg_2[PS_4]$ (**2**)

K_2S_3 (0.093 g, 0.53 mmol), Ag (0.058 g, 0.53 mmol), Nd (0.039 g, 0.27 mmol), P_2S_5 (0.059 g, 0.27 mmol), S (0.051 g, 1.60 mmol) were thoroughly mixed in a N_2-filled glove-box and loaded into fused silica tube which was evacuated (1×10^{-3} mbar) and flame-sealed. The tube was placed in a computer controlled furnace and heated to 700 °C within 24 h. After 5 days the sample was cooled down to 100 °C at a rate of 3 °C/h followed by cooling to room temperature in 4 h. Excess flux was removed by washing the reaction product with dimethylformamide (DMF) and acetone. The product contained transparent colorless platelets $K_3Nd[PS_4]_2$ (~40%) [40] and light yellow platelets $KAg_2[PS_4]$ (~40%). A synthesis of $KAg_2[PS_4]$ was successful reacting stoichiometric amounts of K_2S_3/Ag/P_2S_5 at 700 °C. The product is stable in air for several weeks.

2.4. X-ray crystallography

Data sets of selected crystals of both compounds were collected on a STOE imaging plate diffraction system (IPDS-1) with graphite monochromatized Mo$K\alpha$ radiation ($\lambda = 0.7107$ Å) at room temperature for **1** and at −100 °C for **2**. Size of crystal **1**: $0.13 \times 0.09 \times 0.07$ mm^3; crystal **2**: $0.12 \times 0.10 \times 0.07$ mm^3. The raw intensities were corrected for Lorentz, polarization and absorption. The structures were solved with direct methods and refined with full matrix least squares techniques using the SHELXTL software package [57].

2.4.1. $Ag_2Nb[P_2S_6][S_2]$

The structure was solved and refined successfully in space group *Pnma*. The final cycle of refinement performed with 1923 unique reflections converged to residuals wR_2 ($F_o^2 > 0$) = 0.0975 and the conventional R index based on reflections $F_o^2 > 2\sigma$ (F_o^2) was 0.0380. The resulting structural models of both compounds were standardized using the program STRUCTURE TIDY [58] in PLATON [59].

2.4.2. $KAg_2[PS_4]$

The systematic absence conditions of the data set pointed to eight possible space groups. The three choices with the lowest CFOM (combined figure of merit) were $I\bar{4}$ (acentric), $I\bar{4}2m$ (acentric) and $I4/m$ (centrosymmetric). The intensity statistics indicated a non-centrosymmetric space group. Therefore, we first proceeded with $I\bar{4}2m$ since it belongs to the higher symmetric Laue class ($4/mmm$). All atoms were found with two runs of least-squares/difference Fourier cycles. In the initial stages of the refinement, the incorrect enantiomorphs (wrong absolute structure) were selected; therefore the coordinates were inverted with the instruction MOVE 1 1 1 −1 and subsequently refined anisotropically. After introducing an extinction coefficient, the R values dropped significantly to $R1 = 0.0336$ and w$R2 = 0.0893$. The absolute structure was determined and is in agreement with the selected setting (Flack x parameter: −0.1(1)). The structure is clearly non-centrosymmetric with no additional mirror planes perpendicular to the c-axis and could not be solved in the centrosymmetric space group $I4/m$. An attempt to solve the structure in the non-centrosymmetric space group $I\bar{4}$ showed reasonable results. But a symmetry check with PLATON [59] suggests the higher symmetry space group $I\bar{4}2m$.

The parameters for data collection and the details of the structural refinements for the two compounds are summarized in Table 1. Atomic coordinates and isotropic displacement parameters are given in Table 2. Selected bond distances and angles are listed in Tables 3 (**1**) and 4 (**2**).

Table 1
Crystal data and selected refinement results for $Ag_2Nb[P_2S_6][S_2]$ (**1**) and $KAg_2[PS_4]$ (**2**).

	$Ag_2Nb[P_2S_6][S_2]$	$KAg_2[PS_4]$
fw	627.15	414.05
Space group	*Pnma*	$I\bar{4}2m$
a (Å)	12.2188 (11)	6.6471 (7)
b (Å)	26.3725 (16)	6.6471 (7)
c (Å)	6.7517 (4)	8.1693 (11)
V (Å^3)	2572.7 (3)	360.95(7)
Z	8	2
T (K)	170	293
D_{calc} (g cm^{-3})	3.829	3.810
μ (mm^{-1})	6.371	7.263
Index range	$-13 \leqslant h \leqslant 14$	$-8 \leqslant h \leqslant 8$
	$-31 \leqslant k \leqslant 31$	$-8 \leqslant k \leqslant 8$
	$-7 \leqslant l \leqslant 7$	$-10 \leqslant l \leqslant 10$
$2\Theta_{max}$ (°)	55	56
R_{int}	0.0446	0.0436
$R1(F_o > 4\sigma(F_o))$	0.0380	0.0336
w$R2$ (all data)	0.0975	0.0893
GOOF	0.983	1.196
$\Delta\rho$ [e Å^{-3}]	1.965/−1.932	1.257/−1.166

$R1 = \sum||F_o|-|F_c||/\sum|F_o|$.
w$R2 = [\sum w(F_o^2-F_c^2)^2/\sum w(F_o^2)^2]^{1/2}$, $w = 1/[\sigma(F_o^2)+(a^*P)^2+b^*P]$, where $P = (\max(F_o^2,0)+2F_c^2)/3$.

Table 2
Atomic coordinates and equivalent displacement parameters U_{eq} ($Å^2 \times 10^3$).

	x	y	z	U_{eq}
$Ag_2Nb[P_2S_6][S_2]$				
Ag(1)	0.08482(7)	0.05458(3)	0.01326(12)	36(1)
Ag(2)	0.14926(6)	0.04371(3)	0.50780(10)	24(1)
Nb(1)	0.36746(5)	0.19556(2)	0.46668(9)	4(1)
P(1)	0.10680(15)	0.60636(7)	0.3074(3)	5(1)
P(2)	0.34241(15)	0.10707(7)	0.1257(3)	5(1)
S(1)	0.00499(14)	0.66453(6)	0.2510(3)	7(1)
S(2)	0.03093(15)	0.53747(7)	0.2804(3)	9(1)
S(3)	0.24340(14)	0.62128(7)	0.1479(3)	7(1)
S(4)	0.24167(14)	0.16593(7)	0.1764(3)	7(1)
S(5)	0.26540(15)	0.03929(7)	0.1737(3)	10(1)
S(6)	0.48122(14)	0.12282(6)	0.2765(3)	8(1)
S(7)	0.0351(2)	$\frac{1}{4}$	0.0604(4)	9(1)
S(8)	0.2002(2)	$\frac{1}{4}$	0.4996(5)	8(1)
S(9)	0.2977(2)	$\frac{1}{4}$	0.7404(4)	8(1)
S(10)	0.4388(2)	$\frac{1}{4}$	0.1957(4)	9(1)
$KAg_2[PS_4]$				
Ag	0	$\frac{1}{4}$	$\frac{1}{4}$	35(1)
K	0	0	$\frac{1}{2}$	18(1)
P	0	0	0	8(1)
S	0.18131(18)	0.18131(18)	0.1398(2)	15(1)

Estimated deviations are given in parentheses. The U_{eq} is defined as one third of the trace of the orthogonalized *Uij* tensor.

Table 3
Selected distances (Å) and angles (deg) for $Ag_2Nb[P_2S_6][S_2]$ (**1**).

Ag(1)–S(2)	2.4771(19)	Ag(1)–S(5)	2.491(2)
Ag(1)–S(6)	2.6185(19)	Ag(2)–S(3)	2.6077(18)
Ag(2)–S(2)	2.6305(19)	Ag(2)–S(5)	2.667(2)
Ag(2)–S(5)	2.671(2)	Nb(1)–S(10)	2.483(2)
Nb(1)–S(9)	2.491(2)	Nb(1)–S(7)	2.508(2)
Nb(1)–S(8)	2.508(2)	Nb(1)–S(1)	2.6044(18)
Nb(1)–S(4)	2.6104(18)	Nb(1)–S(3)	2.6776(18)
Nb(1)–S(6)	2.6947(18)	Nb(1)–Nb(1)	2.8714(13)
P(1)–S(1)	2.011(3)	P(1)–S(3)	2.025(3)
P(1)–S(2)	2.048(3)	P(1)–P(2)	2.237(3)
P(2)–S(4)	2.010(2)	P(2)–S(6)	2.021(3)
P(2)–S(5)	2.046(3)	P(2)–P(1)	2.237(3)
S(8)–S(9)	2.016(4)	S(10)–S(7)	2.023(4)
S(2)–Ag(1)–S(5)	145.53(7)	S(2)–Ag(1)–S(6)	106.45(6)
S(5)–Ag(1)–S(6)	107.68(6)	S(3)–Ag(2)–S(2)	105.83(6)
S(3)–Ag(2)–S(5)	94.21(6)	S(2)–Ag(2)–S(5)	154.45(6)
S(3)–Ag(2)–S(5)	107.12(6)	S(2)–Ag(2)–S(5)	92.72(6)
S(5)–Ag(2)–S(5)	96.38(4)	S(10)–Nb(1)–S(9)	109.48(5)
S(10)–Nb(1)–S(7)	47.83(8)	S(9)–Nb(1)–S(7)	90.20(7)
S(10)–Nb(1)–S(8)	91.17(7)	S(9)–Nb(1)–S(8)	47.58(8)
S(7)–Nb(1)–S(8)	110.14(5)	S(10)–Nb(1)–S(1)	120.96(7)
S(9)–Nb(1)–S(1)	80.73(7)	S(7)–Nb(1)–S(1)	75.22(7)
S(8)–Nb(1)–S(1)	127.04(7)	S(10)–Nb(1)–S(4)	80.02(7)
S(9)–Nb(1)–S(4)	121.89(7)	S(7)–Nb(1)–S(4)	126.69(8)
S(8)–Nb(1)–S(4)	75.99(7)	S(1)–Nb(1)–S(4)	144.26(6)
S(10)–Nb(1)–S(3)	159.58(7)	S(9)–Nb(1)–S(3)	84.81(6)
S(7)–Nb(1)–S(3)	149.92(7)	S(8)–Nb(1)–S(3)	88.05(6)
S(1)–Nb(1)–S(3)	74.70(5)	S(4)–Nb(1)–S(3)	79.99(6)
S(10)–Nb(1)–S(6)	83.07(5)	S(9)–Nb(1)–S(6)	160.13(7)
S(7)–Nb(1)–S(6)	87.22(6)	S(8)–Nb(1)–S(6)	150.49(7)
S(1)–Nb(1)–S(6)	79.56(6)	S(4)–Nb(1)–S(6)	74.50(6)
S(3)–Nb(1)–S(6)	87.59(6)	S(10)–Nb(1)–Nb(1)	54.68(4)
S(9)–Nb(1)–Nb(1)	54.80(4)	S(7)–Nb(1)–Nb(1)	55.07(4)
S(8)–Nb(1)–Nb(1)	55.08(4)	S(1)–Nb(1)–Nb(1)	108.31(4)
S(4)–Nb(1)–Nb(1)	107.42(4)	S(3)–Nb(1)–Nb(1)	137.02(4)
S(6)–Nb(1)–Nb(1)	135.39(4)	S(1)–P(1)–S(3)	105.12(11)
S(1)–P(1)–S(3)	105.12(11)	S(1)–P(1)–S(2)	112.33(11)
S(3)–P(1)–S(2)	119.88(11)	S(1)–P(1)–P(2)	110.32(11)
S(3)–P(1)–P(2)	106.29(10)	S(2)–P(1)–P(2)	102.61(10)
S(4)–P(2)–S(6)	105.62(11)	S(4)–P(2)–S(5)	111.47(11)
S(6)–P(2)–S(5)	119.05(11)	S(4)–P(2)–P(1)	109.87(10)
S(6)–P(2)–P(1)	104.64(10)	S(5)–P(2)–P(1)	105.83(10)

Table 4
Selected distances (Å) and angles (deg) for $KAg_2[PS_4]$ (**2**).

Ag–S	$2.5980(7) \times 4$	P–S	$2.0519(16) \times 4$
K–S	$3.2062(18) \times 4$	K–S	$3.4003(18) \times 4$
S–Ag–S	$96.89(2) \times 4$	S–Ag–S	$139.47(7) \times 2$
S–P–S	$112.34(10) \times 2$	S–P–S	$108.06(5) \times 4$
P–S–Ag	$113.53(3) \times 2$	Ag–S–Ag	129.53(6)

Further details of the crystal structure investigation can be ordered referring to the no. CSD-420032 ($Ag_2Nb[P_2S_6][S_2]$), CSD-420033 ($KAg_3[PS_4]$), the authors and the citation of this paper at the Fachinformationszentrum Karlsruhe, Gesellschaft für wissenschaftlich-technische Information mbH. D-76344 Eggenstein-Leopoldshafen (Germany). E-mail: crysdata@fiz-karlsruhe.de

2.5. Physical measurements

2.5.1. Infrared spectroscopy

Infrared spectra in the MIR region (4000–400 cm^{-1}, 2 cm^{-1} resolution) were recorded on a Genesis FT-spectrometer (ATI Mattson). The samples were ground with dry KBr into fine powders and pressed into transparent pellets. Infrared spectra in the far-IR region (550–80 cm^{-1}) were collected on an ISF-66 device (Bruker) with the samples pressed in polyethylene pellets.

2.5.2. Raman spectroscopy

Raman spectra were recorded on an ISF-66 spectrometer (Bruker) equipped with an additional FRA 106 Raman module. An Nd/YAG laser was used as source ($\lambda = 1064$ nm). The samples were ground and prepared on Al sample holders. The measuring range was −1000–3500 cm^{-1} (resolution: 2 cm^{-1}).

2.5.3. Solid-state ultraviolet (UV)–visible (vis)–near-IR (NIR) spectroscopy

Optical diffuse reflectance measurements were performed at room temperature using a UV–vis–NIR two-channel spectrometer Cary 5 from Varian Techtron Pty., Darmstadt. The spectrometer is equipped with an Ulbricht sphere (Diffuse reflectance accessory; Varian Techtron Pty.). The inner wall of the Ulbricht sphere (diameter 110 mm) is covered with a PTFE layer of 4 mm thickness. A PbS detector (NIR) and a photomultiplier (UV/vis) are attached to the Ulbricht sphere. The samples were ground with $BaSO_4$ (as standard for 100% reflectance) and prepared as a flat specimen. The resolution was 1 nm for the UV/vis range and 2 nm for the NIR range. The measuring range was 250–2000 nm. Absorption (α/S) data were calculated from the reflectance spectra using the Kubelka–Munk function [60]: $\alpha/S = (1-R)^2/2R$, where R is the reflectance at a given wave-number, α is the absorption coefficient and S is the scattering coefficient. The band gap was determined as the intersection point between the energy axis at the absorption offset and the line extrapolated from the linear part of the absorption edge in a $(\alpha/S)^2$ vs. E (eV) plot.

2.5.4. Microprobe analyses

Microprobe analyses were performed with a Philips ESEM XL 30 scanning electron microscope equipped with an EDAX analyzer. The compositions are the result of averaging a large

number of independent measurements from a given sample. The EDX data yielded an atomic ratio of 1.7:1:1.8:7.6 (Ag:Nb:P:S) for compound **1** and 1:2:1:3.7 (K:Ag:P:S) for compound **2**.

3. Results and discussion

3.1. Syntheses and crystal structures

3.1.1. $Ag_2Nb[P_2S_6][S_2]$ (**1**)

A view of the structure of compound **1** is presented in Fig. 1. The structure is characterized by a strongly anisotropic three-dimensional framework composed of three types of slabs. The framework can be conveniently described as an assembly of $[Nb_2S_{12}]$ units running along the [010] direction, ethane-like $[P_2S_6]$ groups and novel $[Ag_2S_4]$ chains. The $[Nb_2S_{12}]$ units are not directly joined, but they are connected via the $[P_2S_6]^{4-}$ anions along [001] to form intricate chains which contain 14-membered rings (Fig. 2). Neighboring chains are linked through $[Ag_2S_4]$ chains creating tunnels (diameter: 3.6×10.3 Å) along [001], whereas $[P_2S_6]$ units and $[Ag_2S_4]$ chains form tunnels with dimensions of 3.6×6.5 Å in-between. The latter tunnels are compact and define uniform slabs of almost constant thickness, which constitute the central part of the framework. The $[Nb_2S_{12}]$ units are grafted alternatively on both sides of these slabs. In the $[Nb_2S_{12}]$ unit, both Nb atoms are surrounded by eight S atoms in a distorted bicapped trigonal prismatic fashion as shown in Fig. 3. Two adjacent NbS_8 trigonal prisms share a rectangular face of two S_2^{2-} pairs; the two other rectangular faces are capped by S atoms from $[P_2S_6]^{4-}$ anions. The S–S bonds of the $[S_2]$ groups, 2.016(4) and 2.023(4) Å, are characteristic for S_2^{2-} anions. The Nb atoms are slightly off-centered, displaced towards the S_2^{2-} anions and moved away from the $[Ag_2S_4]$ chains and $[P_2S_6]^{4-}$ anions. Indeed, the shortest Nb–S bonds (Nb–S(7, 8, 9, 10): 2.483(2)–2.508(2) Å) are to the S atoms of the S_2^{2-} pairs. The Nb–S bonds involving S atoms having bonds to both Ag and P atoms are the longest (Nb–S(3, 6): 2.6776(18), 2.8714(18) Å), whereas those to S atoms which are only bound to P atoms are in-between (Nb–S(1, 4): 2.6044(18); 2.6104(18) Å). However, the average Nb–S distance of 2.572(2) Å compares well with the value of 2.550(2) Å in $NaNb_2PS_{10}$ [22,47]. The presence of Nb^{IV} $4d^1$ leads to a short Nb–Nb distance of 2.8714(13) Å, being comparable to those in NbP_2S_8 [45,46], ANb_2PS_{10} (A = Na, Ag, K, Rb, Cs) [22,47–50], $K_{0.5}Ag_{0.5}Nb_2PS_{10}$ [51], $Rb_{0.38}Ag_{0.5}Nb_2PS_{10}$ [52] and $K_{0.34}Cu_{0.5}Nb_2PS_{10}$ [53]. The tetracapped trigonal $[Nb_2S_{12}]$ biprisms share four opposite edges with $[P_2S_6]$ entities to build alternating chains parallel to [001] (Figs. 1 and 2).

The $[Nb_2S_{12}]$ unit is a central structural motif in 2D-NbP_2S_8 [46], 3D-NbP_2S_8 [45], Nb_2PS_{10} [43] and $Nb_4P_2S_{21}$ [44]. The formation of this building block may be mainly due to the stabilization of the $4d^1$ electronic configuration of Nb^{IV} by a D_{3h} symmetry crystal field, as for V^{IV} $3d^1$ in V_2PS_{10} [61]. On the other hand the presence of S_2^{2-} dumb-bells allows that the Nb^{IV} centers can come in close contact. In all reported $[Nb_2S_{12}]$ units, the Nb–Nb distances are very similar independent of the number of S_2 pairs present in the actual structure: two [46] or four [43,44,48]. This distance is almost unchanged in isotypic $[Nb_2X_{12}]$ groups like

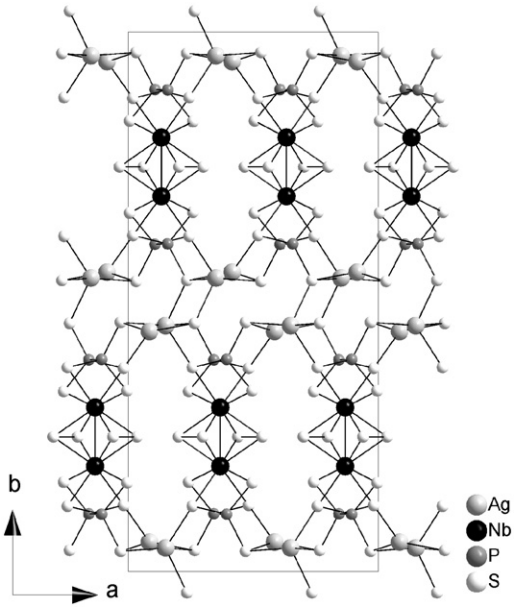

Fig. 1. Perspective view of $Ag_2Nb[P_2S_6][S_2]$ (**1**) along [001].

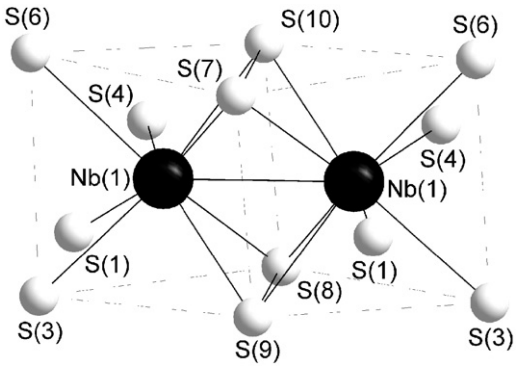

Fig. 3. A side view of tetracapped trigonal biprisms $[Nb_2S_{12}]$ with atomic labeling.

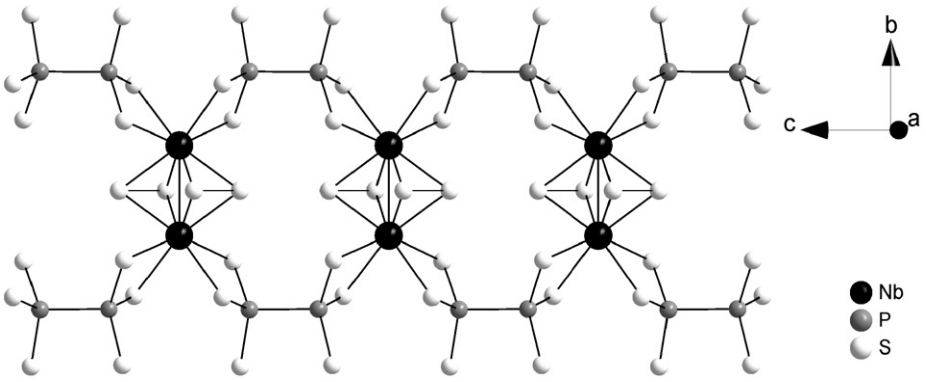

Fig. 2. Perspective view of a single $[NbP_2S_8]^{2n-}$ chain.

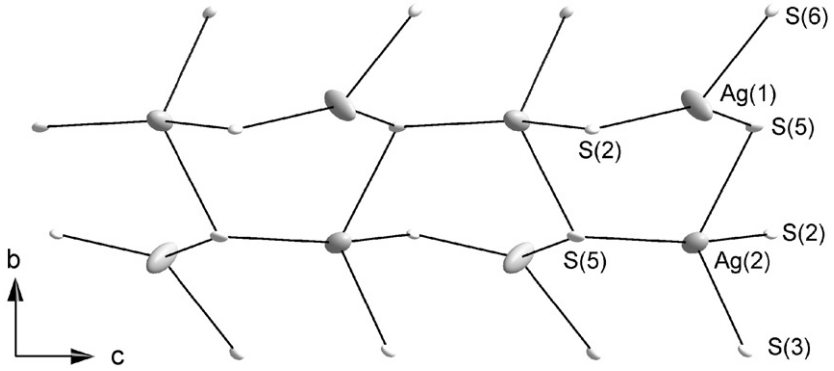

Fig. 4. View of the $[Ag_2S_4]$ chain along [001]. Displacement ellipsoids are drawn at the 50% probability level.

in NbS_2Cl_{12} (2.871(4) Å) [62,63] or Nb_2Se_9 (2.895(2) Å) [64]. Like in the other compounds mentioned above, the neighbored Nb atoms form an isolated pair via a single Nb–Nb bond.

The ethane-like $[P_2S_6]^{4-}$ anion in staggered conformation is the second basic building block of the structure and is composed of two $[PS_3]$ units sharing the vertex with each other to form a P–P bond of 2.237(3) Å. The P–S bond lengths range from 2.011(3) to 2.048(3) Å (average: 2.027(3) Å) being in good agreement with data reported for $M_2P_2S_6$ (M = Cd, Zn, Mn, Fe, Co, Ni, Hg, Mg, Ca, V, Pd, Sn) [2–9]. However, a thorough analysis of the P–S bond lengths and the S–P–S angles reveals that the P(1,2) atoms are slightly displaced from the centres of the tetrahedra yielding three groups of P–S bond lengths: (i) the P(1)–S(1) and P(2)–S(4) bonds of 2.011(3) and 2.010(2) Å where the S atoms have bonds to a Nb atom; (ii) the P(1)–S(3) and P(2)–S(6) bonds of 2.025(3) and 2.021(3) Å with S atoms being involved in bonds to Nb and Ag atoms; (iii) the P(1)–S(2) and P(2)–S(5) bonds of 2.048(3) and 2.046(3) Å with S atoms having also bonds to Ag^+ ions. The S–P–S angles indicate an obvious deviation from the tetrahedral geometry (see Table 3).

The new puckered $[Ag_2S_4]$ chain (Fig. 4) is the third building block and is formed by $Ag(1)S_3$ triangles and $Ag(2)S_4$ tetrahedra. Each $Ag(1)S_3$ triangle shares the S(2) atom with one $Ag(2)S_4$ tetrahedron and the S(5) atom with two other $Ag(2)S_4$ tetrahedra, while each $Ag(2)S_4$ tetrahedron shares two S(5) atoms with neighboring $Ag(1)S_3$ triangles and $Ag(2)S_4$ tetrahedra and the S(2) atom with one $Ag(1)S_3$ triangle. The remaining S(3) and S(6) atoms have bonds to Nb and P(2). Two $Ag(1)S_3$ triangles and two $Ag(2)S_4$ tetrahedra are connected to form one six-membered ring. The chains containing six-membered rings run along the [001] direction. Both Ag^+ ions are ordered in contrast to the disorder observed in $Ag_2NbTi_2P_6S_{25}$ [21]. The $Ag(1)S_3$ triangle is slightly distorted with Ag(1)–S(2, 5, 6) bonds at 2.4771(19), 2.491(2), 2.6185(18) Å and S–Ag–S angles between 106.45(6) and 145.53(7)°. Ag(2) is in a strong distorted tetrahedral coordination with Ag(2)–S bond lengths ranging from 2.6077(18) to 2.671(2) Å and corresponding angles between 92.72(6)° and 154.45(6)°.

Analyzing the anisotropic displacement parameters (ADP) it is obvious that Ag(1) exhibits the largest values for the ADP. Despite that S(2) and S(5) serve as bridges within the chain and the Ag(1)–S(2, 5) bonds are shorter than all Ag(2)–S bonds, the ADPs of Ag(1) are larger. A possible explanation is the environment of Ag(1) in the center of a plane made by three S atoms that allows an unconstrained vibration perpendicular to the triangle.

The bridging S(2) atom connects two Ag^+ ions with an Ag–S–Ag angle of 86.89(6)°, whereas S(5) links three Ag^+ with Ag–S–Ag angles ranging from 83.65(6)° to 126.74(7)°. The average Ag–S bond length is 2.59 Å comparable with that found in KAg_2PS_4 (see below).

Within the chain short and long Ag–Ag separations of 3.4425(11) and 3.5141(11) Å alternate. With the usual oxidation states for Ag, Nb and P and taking into account the S_2^{2-} anion, a straightforward charge balance $(Ag^{+1})_2(Nb^{+4})(P^{+4})_2(S^{-2})_6(S_2)^{2-}$ is achieved.

Obviously, the structure of compound **1** is completely different from that of $AgNb_2PS_{10}$ [22,47] and $K_{0.5}M_{0.5}Nb_2PS_{10}$ (M = Cu, Ag) [51,53]. In $AgNb_2PS_{10}$ and $K_{0.5}Ag_{0.5}Nb_2PS_{10}$, the $[Nb_2S_{12}]$ groups are connected via $[PS_4]$ units and S_2 dumbbells to form $^1_\infty[Nb_2PS_{10}]^-$ chains. The $[PS_4]^{3-}$ anions bridge the Nb–Nb pair with the long separation. Ag^+ is in a distorted tetrahedral environment with two short Ag–S (2.545(4), 2.624(3) Å) and two long bonds (2.872(4), 2.898(3) Å). This Ag–S bonding pattern is similar to that in the AgS_4 tetrahedra in both title compounds.

Attempts to prepare the analogous Cu compound yielded NbP_2S_8 [45,46]. This observation suggests that the ionic radius of Cu is too small to stabilize the three-dimensional framework of **1**.

3.1.2. $KAg_2[PS_4]$ (**2**)

Initially the syntheses were performed with the aim to prepare new lanthanide (Nd) alkali-metal silver thiophosphates via the flux method. Compound **2** was obtained in a reasonable yield by reacting a mixture of K_2S_3/Ag/Nd/P_2S_5/S with molar ratio of 2/2/1/1/6. Decreasing the amount of Ag leads to the formation of $K_3Nd[PS_4]_3$ as main product. The reaction without Nd was also explored, and under the same conditions, compound **2** could be obtained.

The structure is composed of a three-dimensional anionic framework with orthogonal, intersecting tunnels hosting the K^+ cations. These tunnels run parallel to the [100] and [010] directions. In the asymmetric unit there are one K and P atom, both located on $\bar{4}2m$ sites, one Ag atom on $\bar{4}$ and an S atom on a mirror plane. The anionic framework is constructed by corner-sharing of alternating $[PS_4]$ and $[AgS_4]$ tetrahedra, forming a flattened eight-membered ring (Fig. 5). The $[PS_4]$ tetrahedron is regular, with all bonds at 2.519(16) Å and bond angles between 108.06(5) and 112.34(10)°. The $[AgS_4]$ tetrahedron is severely distorted with bond angles from 96.89(2) to 139.47(7)°, even though all Ag–S bond lengths are 2.5980(7) Å. The orthogonal rings, perpendicular to the [100] and [010] directions, are connected through P and S atoms to form a three-dimensional body-centered framework. Every S atom is three coordinated to one P and two Ag atoms. The structure can also be described as layers of corner-sharing $[AgS_4]$ tetrahedra combined to eight-membered rings parallel to the (001) plane. These layers are

stitched by $[PS_4]$ tetrahedra along the [001] direction to form the three-dimensional framework. The tunnels accommodate the K^+ cations, which are coordinated by eight S atoms in a compressed cube, with K–S distances from 3.2062(18) to 3.4003(18) Å (Table 4). The dimension of the tunnels is about 4.08×6.65 Å measured from coordinate to coordinate.

We note that compound **2** is isostructural with KAg_2AsS_4 [65], KAg_2SbS_4 [66], $(NH_4)Ag_2AsS_4$ [67] and $BaAg_2GeS_4$ [68]. The structure of these compounds can be derived from the ZnS sphalerite-type structure. The chalcopyrite structure-type ($CuFeS_2$ [69]) in space group $I\bar{4}2d$ is an ordered superstructure of ZnS with the Zn atoms being replaced alternatively by Cu and Fe in a regular fashion. It is also possible that one type of cation is distributed over two different crystallographic sites whereas the other cation being located on only one site. But in this case the symmetry will be reduced to $I\bar{4}2m$. For example, in Cu_3SbS_4 [70], two-thirds of Cu are located on one crystallographic site, while one-third sits on another site; and Sb is on the third site. From sphalerite to chalcopyrite, a small distortion along the *c*-axis, known as a tetragonal compression, is observed. The reason is the difference of the radii of two cations that make the unit cell height slightly less than twice the base dimensions. The ratio *c*/*a* (better 2-*c*/*a*) is a measure of the tetragonal distortion. The 2-*c*/*a* values for $CuFeS_2$ (0.03), $AgGaS_2$ (0.14), AgGaSe2 (0.11), $AgInS_2$ (0.05) [71], $CuInSe_2$ (0) [72], Cu_3SbS_4 (0) [70] are small or zero. Since the cationic radii in these compounds are very similar, they can be viewed as relatively ideal derivatives of the chalcopyrite structure-type. Larger 2-*c*/*a* values are found for compound **2** (0.77), KAg_2AsS_4 (0.78) [65], KAg_2SbS_4 (0.78) [66], $(NH_4)Ag_2AsS_4$ (0.78) [67] and $BaAg_2GeS_4$ (0.83) [44]. The *c*-axis compression expands the coordination number of one of the cations from 4 to 8. This is the reason why these compounds containing non-tetrahedral cations can adopt this structure type. In fact, in all of these compounds K^+, NH_4^+, Ba^{2+} occupy the large cation site whose coordinate number is 8 instead of 4. P, As, Ge occupy the regular tetrahedral site, while the remaining highly distorted tetrahedral site is occupied by the Ag^+ cation.

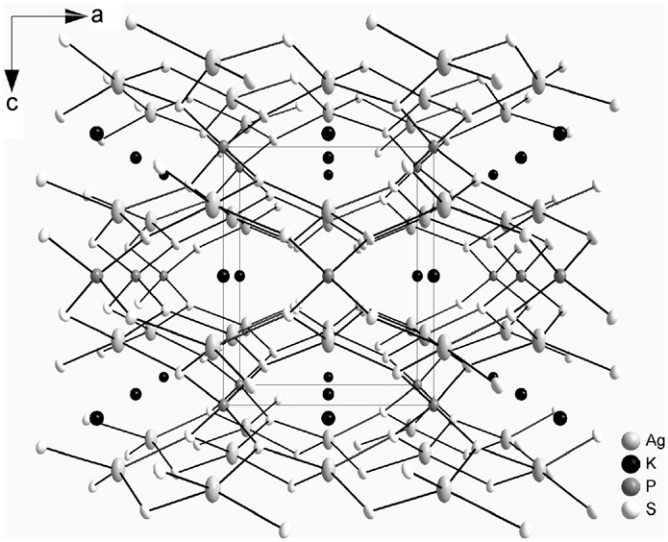

Fig. 5. Perspective view of the structure of $KAg_2[PS_4]$ viewed along [010]. Displacement ellipsoids are drawn at the 50% probability level for Ag, K and S atoms, 80% for P atoms.

3.2. Optical properties

The solid state diffuse reflectance UV/vis spectra of compounds **1** and **2** (Fig. 6) show steep absorption edges and the band gaps E_g are estimated to 2.02 eV for **1** and 3.02 eV for **2**. These data are in agreement with the transparent colorless (**2**) and red color (**1**) of the samples.

The MIR and Raman spectra for **1** are shown in Fig. 7. The spectroscopic relevant units are bridging S_2^{2-} dumbbells between Nb atoms and $[P_2S_6]^{4-}$ anions with approximate D_{3d} symmetry. For $[P_2S_6]^{4-}$ the following modes can be expected: $\Gamma_{vib}(D_{3d}) = 3A_{1g}(R)+3E_g(R)+A_{1u}+2A_{2u}(IR)+3E_u(IR)$, where the *gerade* species are Raman active and *ungerade* species, except A_{1u}, are infrared active. On the basis of the assignment of the Raman bands for hexathiodiphosphates [23,73,74], the modes observed for the title compound are assigned. The peaks above 150 cm^{-1} in the Raman spectrum correspond to the modes of the $[P_2S_6]^{4-}$ anions, whereas the peaks below 150 cm^{-1} may be explained with the modes with participation of metal ions. Compared to the spectra of hexathiodiphosphates [23,73,74] and $Li_4[P_2S_6]$ [75], the band at 384 cm^{-1} is assigned to the A_{1g} mixed symmetric P–P and P–S stretching modes, while the resonances in the 150–350 cm^{-1} region may be caused by the $[P_2S_6]^{4-}$ deformation or bending vibrations (S–P–S and S–P–P modes (E_g)). The mode at 431 cm^{-1} in the Raman spectrum (438 cm^{-1} in the IR) is assigned to an A_{2u} vibrational mode. This peak is normally only IR active, but due to the missing inversion center between two P atoms in $Ag_2Nb[P_2S_6][S_2]$, the $[P_2S_6]^{4-}$ unit does not have idealized D_{3d} symmetry. This allows the A_{2u} peak to be observed in the Raman spectrum.

Analogous to $Nb_2(S_2)_2Cl_4$ [76], the weak resonance at 542 cm^{-1} in the Raman spectrum and the peaks at 537 and 593 cm^{-1} are attributed to the S–S stretching vibration. The remaining signals at 632 and 569 cm^{-1} in the IR spectrum and the peaks at 630, 616 and 572 cm^{-1} may be caused by P–S stretching vibrations.

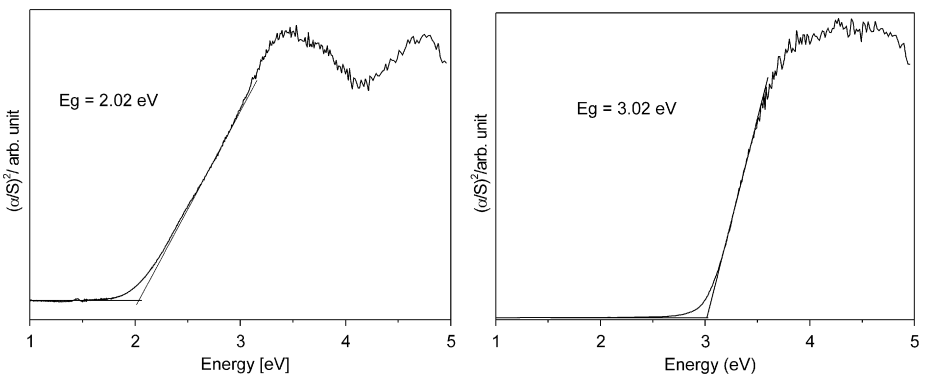

Fig. 6. Transformed reflectance spectra of $Ag_2Nb[P_2S_6][S_2]$ (**1**) (left) and $KAg_2[PS_4]$ (**2**) (right).

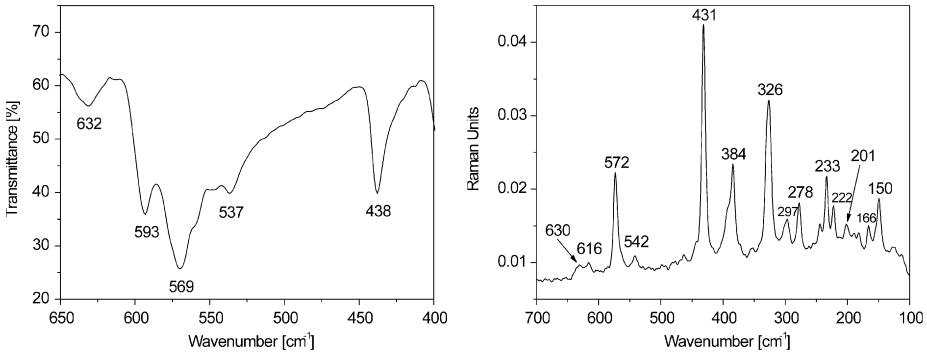

Fig. 7. MIR and FT-Raman spectra of $Ag_2Nb[P_2S_6][S_2]$ (**1**).

Both Raman and IR assignments for the $[P_2S_6]^{4-}$ unit correspond well with those reported for $K_2Fe[P_2S_6]$ [77], $KLa[P_2S_6]$ [78] and $Cr_4[P_2S_6]_3$ [23].

4. Conclusions

The two new compounds $Ag_2Nb[P_2S_6][S_2]$ and $KAg_2[PS_4]$ crystallize in two different three-dimensional frameworks. The compressed chalcopyrite related structure adopted by $KAg_2[PS_4]$ indicates that compounds containing large alkali ions which prefer high coordination numbers can be accommodated in this structure type. The flexibility of this structure type could be useful in modifying the properties of the material. It is also imaginable to predict other possible quaternary silver sulfides and selenides that might adopt the same structure type. In $Ag_2Nb[P_2S_6][S_2]$, the framework is constructed by $[Nb_2S_{12}]$ units linked through $[P_2S_6]$ units and the new $[Ag_2S_4]$ chains built up from distorted $[AgS_3]$ triangles and $[AgS_4]$ tetrahedra. In KAg_2PS_4 the Ag^+ ion is in a distorted tetrahedral environment whereas in $Ag_2Nb[P_2S_6][S_2]$ two different polyhedra are observed for Ag^+. The occurrence of Ag–Ag bonds could be ruled out, whereas the rather usual feature of coinage elements was observed i.e., large anisotropic displacement parameters (ADP) especially for the AgS_3 triangle in **1**. Large ADPs are often a hint for Ag^+ mobility and the investigation of ionic conductivity will be done in the near future.

Acknowledgments

Financial support by the State of Schleswig-Holstein, the Fonds der Chemischen Industrie (FCI) and DFG (Deutsche Forschungsgemeinschaft) is gratefully acknowledged.

Appendix A. Supplementary material

Supplementary data associated with this article can be found in the online version at 10.1016/j.jssc.2008.11.017.

References

[1] P. Villars, L.D. Calvert, Pearson's Handbook of Crystallographic Data for Intermetallic Compounds and Desk Edition 1997, second ed., ASM, Metals Park, OH, 1997.
[2] F. Boucher, M. Evain, R. Brec, Acta Cryst. B 51 (1995) 952–961.
[3] F. Boucher, M. Evain, R. Brec, J. Alloys Compd. 215 (1994) 63–70.
[4] E. Prouzet, G. Ouvrard, R. Brec, Mater. Res. Bull. 21 (1986) 195–200.
[5] G. Ouvrard, R. Brec, J. Rouxel, Mater. Res. Bull. 20 (1985) 1181–1189.
[6] A.A. El-Meligi, Mater. Chem. Phys. 89 (2005) 253–259.
[7] G. Ouvrard, R. Brec, J. Rouxel, C.R. Acad. Sci. Ser. II 294 (1982) 971–972.
[8] P. Fragnaud, E. Prouzet, R. Brec, J. Mater. Res. 7 (1992) 1839–1846.
[9] W. Klingen, R. Ott, H. Hahn, Z. Anorg. Allg. Chem. 396 (1973) 271–278.
[10] S. Lee, P. Colombet, G. Ouvrard, R. Brec, Inorg. Chem. 27 (1988) 1291–1294.
[11] P. Colombet, S. Lee, G. Ouvrard, R. Brec, J. Chem. Res.-S (1987) 134–135.
[12] P. Colombet, A. Leblanc, M. Danot, J. Rouxel, Nou. J. Chim. New J. Chem. 7 (1983) 333–338.
[13] Z. Ouili, A. Leblanc, P. Colombet, J. Solid State Chem. 66 (1987) 86–94.
[14] M.A. Gave, D. Bilc, S.D. Mahanti, J.D. Breshears, M.G. Kanatzidis, Inorg. Chem. 44 (2005) 5293–5303.
[15] S. Jörgens, A. Mewis, Z. Anorg. Allg. Chem. 630 (2004) 51–57.
[16] A. Van der Lee, F. Boucher, M. Evain, R. Brec, Z. Kristallogr. 203 (1993) 247–264.
[17] M. Evain, F. Boucher, R. Brec, Y. Mathey, J. Solid State Chem. 90 (1991) 8–16.
[18] F. Boucher, M. Evain, R. Brec, Eur. J. Solid State Inorg. Chem. 28 (1991) 383–395.
[19] P. Toffoli, J.C. Rouland, P. Khodadad, N. Rodier, Acta Cryst. C 41 (1985) 645–647.
[20] E. Gaudin, L. Fischer, F. Boucher, M. Evain, V. Petricek, Acta Cryst. B 53 (1997) 67–75.
[21] J. Angenault, X. Cieren, G. Wallez, M. Quarton, J. Solid State Chem. 153 (2000) 55–65.
[22] E.Y. Goh, S.J. Kim, D. Jung, J. Solid State Chem. 168 (2002) 119–125.
[23] Z.L. Huang, J.T. Zhao, J.X. Mi, S.Y. Mao, L.S. Zheng, J. Solid State Chem. 144 (1999) 388–391.
[24] R. Diehl, C.D. Carpentier, Acta Cryst. B 34 (1978) 1097–1105.
[25] D.S. Kyriakos, A.N. Anagnostopoulos, P. Christidis, V. Gountsidou, J. Cryst. Growth 76 (1986) 6–8.
[26] G. Ouvrard, R. Freour, R. Brec, J. Rouxel, Mater. Res. Bull. 20 (1985) 1053–1062.
[27] G. Burr, E. Durand, M. Evain, R. Brec, J. Solid State Chem. 103 (1993) 514–518.
[28] E. Durand, G. Ouvrard, M. Evain, R. Brec, Inorg. Chem. 29 (1990) 4916–4920.
[29] V. Maisonneuve, V.B. Cajipe, C. Payen, Chem. Mater. 5 (1993) 758–760.
[30] V. Maisonneuve, C. Payen, V.B. Cajipe, J. Solid State Chem. 116 (1995) 208–210.
[31] V. Maisonneuve, M. Evain, C. Payen, V.B. Cajipe, P. Molinie, J. Alloys Compd. 218 (1995) 157–164.
[32] S. Coste, E. Gautier, M. Evain, M. Bujoli-Doeuff, R. Brec, S. Jobic, M.G. Kanatzidis, Chem. Mater. 15 (2003) 2323–2327.
[33] S. Coste, E. Kopnin, M. Evain, S. Jobic, R. Brec, K. Chondroudis, M.G. Kanatzidis, Solid State Sci. 4 (2002) 709–716.
[34] E. Kopnin, S. Coste, S. Jobic, M. Evain, R. Brec, Mater. Res. Bull. 35 (2000) 1401–1410.
[35] E. Durand, M. Evain, R. Brec, J. Solid State Chem. 102 (1993) 146–155.
[36] A. Gutzmann, C. Näther, W. Bensch, Acta Cryst. E 61 (2005) I6–I8.
[37] A. Gutzmann, C. Näther, W. Bensch, Acta Cryst. C 60 (2004) I11–I13.
[38] S. Coste, E. Kopnin, M. Evain, S. Jobic, C. Payen, R. Brec, J. Solid State Chem. 162 (2001) 195–203.
[39] V. Derstroff, J. Ensling, V. Ksenofontov, P. Gütlich, W. Tremel, Z. Anorg. Allg. Chem. 628 (2002) 1346–1354.
[40] Y.D. Wu, W. Bensch, Inorg. Chem. 47 (2008) 7523–7534.
[41] T. Komm, T. Schleid, J. Alloys Compd. 418 (2006) 106–110.
[42] T. Schleid, I. Hartenbach, T. Komm, Z. Anorg. Allg. Chem. 628 (2002) 7–9.
[43] R. Brec, P. Grenouilleau, M. Evain, J. Rouxel, Rev. Chim. Miner. 20 (1983) 295–304.
[44] R. Brec, M. Evain, P. Grenouilleau, J. Rouxel, Rev. Chim. Miner. 20 (1983) 283–294.
[45] M. Evain, R. Brec, G. Ouvrard, J. Rouxel, Mater. Res. Bull. 19 (1984) 41–48.
[46] P. Grenouilleau, R. Brec, M. Evain, J. Rouxel, Rev. Chim. Miner. 20 (1983) 628–635.
[47] D. Jung, S.J. Kim, Bull. Korean Chem. Soc. 24 (2003) 739–743.
[48] J. Do, H. Yun, Inorg. Chem. 35 (1996) 3729–3730.
[49] C. Kim, H. Yun, Acta Cryst. C 58 (2002) I53–I54.
[50] J.E. Kwak, C. Kim, H. Yun, J. Do, Bull. Korean Chem. Soc. 28 (2007) 701–704.
[51] Y.W. Dong, S. Kim, H.S. Yun, H. Lim, Bull. Korean Chem. Soc. 26 (2005) 309–311.
[52] Y.W. Dong, S. Kim, H. Yun, Acta Cryst. C 61 (2005) I25–I26.
[53] J.E. Kwak, H. Yun, Bull. Korean Chem. Soc. 29 (2008) 273–275.
[54] A. Gutzmann, W. Bensch, Solid State Sci. 4 (2002) 835–840.
[55] M. Jansen, Angew. Chem. Int. Ed. Engl. 26 (1987) 1098–1110.

[56] M. Barj, G. Lucazeau, G. Ouvrard, R. Brec, Eur. J. Solid State Inorg. Chem. 25 (1988) 449–461.
[57] G.M. Sheldrick, Acta Cryst. A 64 (2008) 112–122.
[58] L.M. Gelato, E. Parthe, J. Appl. Crystallogr. 20 (1987) 139–143.
[59] A.L. Spek, J. Appl. Crystallogr. 36 (2003) 7–13.
[60] P. Kulbelka, F. Munk, Z. Tech. Phys. 12 (1931) 593–601.
[61] R. Brec, G. Ouvrard, Solid State Ionics 9–10 (1983) 481–484.
[62] C. Sourisseau, P. Gard, M. Fouassier, Chem. Phys. 123 (1988) 405–421.
[63] H.G. von Schnering, W. Beckmann, Z. Anorg. Allg. Chem. 347 (1966) 231–239.
[64] S.A. Sunshine, J.A. Ibers, Acta Cryst. C 43 (1987) 1019–1022.
[65] G.L. Schimek, J.W. Kolis, Acta Cryst. C 53 (1997) 991–992.
[66] G.L. Schimek, W.T. Pennington, P.T. Wood, J.W. Kolis, J. Solid State Chem. 123 (1996) 277–284.
[67] M. Auernhammer, H. Effenberger, E. Irran, F. Pertlik, J. Rosenstingl, J. Solid State Chem. 106 (1993) 421–426.
[68] C.L. Teske, Z. Naturforsch. B 34 (1979) 544–547.
[69] S.R. Hall, J.M. Stewart, Acta Cryst. B 29 (1973) 579–585.
[70] A. Pfitzner, S. Reiser, Z. Kristallogr. 217 (2002) 51–54.
[71] A. Chahed, O. Benhelal, H. Rozale, S. Laksari, N. Abbouni, Phys. Status Solidi B 244 (2007) 629–634.
[72] S. Schorr, G. Geandier, Cryst. Res. Technol. 41 (2006) 450–457.
[73] C. Sourisseau, J.P. Forgerit, Y. Mathey, J. Solid State Chem. 49 (1983) 134–149.
[74] A. Grzechnik, V.B. Cajipe, C. Payen, P.F. McMillan, Solid State Commun. 108 (1998) 43–47.
[75] R. Mercier, J.P. Malugani, B. Fahys, J. Douglade, G. Robert, J. Solid State Chem. 43 (1982) 151–162.
[76] A. Müller, W. Jägermann, J.H. Enemark, Coord. Chem. Rev. 46 (1982) 245–280.
[77] W. Carrillo-Cabrera, J. Sassmannshausen, H.G. von Schnering, F. Menzel, W. Brockner, Z. Anorg. Allg. Chem. 620 (1994) 489–494.
[78] C.R. Evenson, P.K. Dorhout, Inorg. Chem. 40 (2001) 2884–2891.